The resolved structure of the extragalactic supernova remnant SNR 4449-1

M. Mezcua,[1][*] A.P. Lobanov,[1]† I. Martí-Vidal,[1,2]

[1] *Max Planck Institute for Radio Astronomy, Auf dem Hügel 69, D-53121 Bonn, Germany*
[2] *Onsala Space Observatory, Chalmers University of Technology, Sweden*

ABSTRACT

We present very long baseline interferometry (VLBI) observations of the milliarcsecond-scale radio structure of the supernova remnant SNR 4449−1 in the galaxy NGC 4449. This young and superluminous remnant was observed at 1.6 GHz ($\lambda = 18$ cm) with the European VLBI Network. The observations confirm earlier identifications of this object with a supernova remnant (SNR) while revealing a somewhat different morphology compared with the structure reported by Bietenholz et al. from VLBI observations at 1.4 GHz. This difference is discussed here in the context of structural sensitivity of both observations. The 1.6 GHz image yields accurate estimates of the size (0.0422 arcsec × 0.0285 arcsec and 0.8 × 0.5 pc) and age ($\sim$55 yr) of SNR 4449−1. With a total flux of 6.1 ± 0.6 mJy measured in the VLBI image, the historical lightcurve of the source can be well represented by a power-law decay with a power index of -1.19 ± 0.07. The SNR exhibits a decline rate of the radio emission of $2.2\% \pm 0.1\%$ yr^{-1} and a radio luminosity of 1.74×10^{35} erg s^{-1}.

Key words: Stars: supernovae: individual: SNR 4449-1 – ISM: supernova remnants – Radio continuum: general.

1 INTRODUCTION

The young and ultraluminous supernova remnant SNR 4449−1 was discovered in the late 1970s (radio, Seaquist & Bignell 1978; optical, Balick & Heckman 1978) in the star-forming galaxy NGC 4449. NGC 4449 is a barred Magellanic-type irregular galaxy hosting a number of areas of extensive star formation (Reines et al. 2008). The galaxy is located at an estimated distance of 3.82 ± 0.27 Mpc (Annibali et al. 2008).

The SNR 4449−1 was identified as a young and very luminous oxygen-rich supernova remnant (SNR) embedded in an HII region (Blair & Fesen 1998), based on observations in several different wavebands. It was first discovered as a bright, unresolved non-thermal radio source ($\sim$10 mJy at 2.7 GHz; Seaquist & Bignell 1978) located approximately 1 arcmin north of the nucleus of NGC 4449. A steep spectral index $\alpha = -0.95 \pm 0.35$[1] (Seaquist & Bignell 1978) in the radio band and observations of both broad and narrow lines in the optical spectrum (Balick & Heckman 1978) indicated that the source was a SNR.

SNR 4449−1 is one of the few known intermediate-age SNRs,

with an age between that of Cas A ($\sim$330 yrs; Thorstensen et al. 2001) and those of the oldest known extragalactic radio supernovae (SNe), like SN 1923A in M83 (83 yrs; Eck et al. 1998) and SN 1957D, also in M83 (49 yrs; Pennington & Dufour 1983). The SNR in NGC 4449 is also notable as the most luminous and most distant member of the class of oxygen-rich SNRs (Blair et al. 1983). The nature of such a bright luminosity was long suspected to be due to interaction with a surrounding HII region, but *Hubble Space Telescope* (*HST*) observations (Milisavljevic & Fesen 2008) suggested that the remnant is instead interacting with a very dense circumstellar material (CSM) from the SNR's progenitor star of mass $\geqslant 20$ M$_\odot$. The remnant possesses the characteristics of typical SNe of massive stars, since it lies inside a rich cluster of high-mass stars surrounded by a presumably SN- and wind-blown interstellar medium bubble, it is interacting with the dense CSM and it exhibits the chemical properties of an hydrogen-poor envelope progenitor (Milisavljevic & Fesen 2008).

While SNR 4449−1 is currently quite luminous, the significant decline in the remnant's X-ray and radio flux over the last three decades implies that it was even brighter in the past. Lacey et al. (2007) combined newer Very Large Array (VLA) observations of NGC 4449 with archive VLA and Westerbork Synthesis Radio Telescope observations to present the lightcurve of the SNR at 6 and 20 cm from 1973 to 2002. The radio flux of SNR 4449−1 measured at 4.9 GHz has undergone a signficant decline over the last three decades, dropping from 13 to 4 mJy between 1973 and 2002 (Lacey et al. 2007).

---

[*] Email: mmezcua@iac.es
Present address: Instituto de Astrofísica de Canarias, Vía Láctea S/N, La Laguna 38200, Tenerife, Spain
† Visiting Scientist, University of Hamburg / Deutsches Elektronen Synchrotron Forschungszentrum.
[1] The spectral index α is defined here from $S_\nu \propto \nu^\alpha$, where S is the flux density at frequency ν.

SNR 4449−1 was identified with an ultraluminous X-ray source (ULX), NGC 4449-X4, based on *ROSAT* High Resolution Imager (HRI) observations (e.g., Liu & Bregman 2005; Sánchez-Sutil et al. 2006). Application of an absorbed, non-equilibrium ionization model (e.g., Yokogawa et al. 2002) to NGC 4449-X4 yielded an X-ray temperature $T_x \approx 2.2 \times 10^7$ K in the 0.3–8.0 keV band, a column density of $N_H = 1.26 \times 10^{21}$ cm^{-2} and an absorption-corrected luminosity $L_x = 2.3 \times 10^{38}$ erg s^{-1} (Summers et al. 2003). The X-ray temperature measurement was used to estimate an age of ∼270 yrs and an ambient medium density of 120–200 cm^{-3} for this SNR (Summers et al. 2003).

Very long baseline interferometry (VLBI) observations made in 1980 and 1981 with the EVN[2] yielded an upper limit of ⩽ 0.07 arcsec (1.3 pc at 3.82 Mpc) for the angular diameter of SNR 4449−1 (de Bruyn 1983). This upper limit was obtained from interferometric visibilities, while the data were insufficient for obtaining an image. Optical observations with the *HST* in 1996 and 2005 yielded somewhat smaller upper limits of 0.028 arcsec (0.5 pc; Blair & Fesen 1998) and 0.037 arcsec (0.69 pc; Milisavljevic & Fesen 2008), respectively. The expansion velocity of 6000 km s^{-1} obtained from the [OIII] optical emission line (Blair & Fesen 1998) provided an estimated age of the remnant of ∼ 50 yr (Milisavljevic & Fesen 2008). Recently, Bietenholz et al. (2010) reported the first resolved radio image of the remnant, obtained with VLBI and showing two parallel ridge-like structures with an angular extent of 65 mas × 40 mas. Using a slightly larger velocity expansion of 6500 km s^{-1}, they obtained an age estimate of ∼ 70 yrs for the SNR.

We have made a VLBI observation of SNR 4449−1 using the EVN at 1.6 GHz (λ = 18 cm), as part of a larger study of milliarcsecond-scale structure of radio counterparts of ULXs (Mezcua & Lobanov 2011; Mezcua et al. 2013a) identified from a cross-correlation of positions of ULX objects with the FIRST[3] catalogue (Sánchez-Sutil et al. 2006). General results of this study will be described in a forthcoming paper, and here we focus on discussing the properties of milliarcsecond-scale emission in SNR 4449−1.

In Section 2, we describe the EVN observations and data reduction. The resulting image of the millarcsecond-scale structure of radio emission from SNR 4449−1 is presented in Section 3. A discussion given in Section 4 brings these results in the context of long-term evolution of the SNR. We adopt a distance to the SNR of 3.82 Mpc (Annibali et al. 2008), which corresponds to a linear scale of 18.4 pc arcsec^{-1}.

2   OBSERVATIONS AND DATA REDUCTION

SNR 4449−1 in NGC 4449 was observed during a 12 h observing run, during which two other ULXs were also observed, on 2009 June 1 using the EVN at 1.6 GHz (wavelength of 18 cm). Nine EVN antennas participated in the observations, and their basic technical parameters are listed in Table 1.

The observations were made in the phase-referencing mode, with the compact radio source J1221+4411, located ∼1° away from the target, used as a phase calibrator. Observing scans on J1221+4411 and SNR 4449–1 were interleaved, with a calibrator–target cycle time of 8 min (2 min on the phase calibrator

Table 1. Technical characteristics of the EVN observations

Participating telescopes			
Antenna	D (m)	SEFD (Jy)	σ_n (mJy)
Effelsberg (DE)	100	19	...
Jodrell Bank (UK)	76	44	0.24
Medicina (IT)	32	600	0.87
Noto (IT)	32	780	1.00
Onsala (SE)	25	320	0.64
Shanghai (CN)	25	670	0.92
Torun (PL)	32	230	0.54
Urumqi (CN)	25	270	0.58
Westerbork (NL)	83[a]	30	0.20

Notes. D – antenna diameter; SEFD – system equivalent flux density (an integral measure of antenna sensitivity); σ_n – rms noise for 1 min integration on the baseline between the given antenna and Effelsberg; [a] – equivalent antenna diameter for a phased array of 11×25 m antennas used for the observations.

and 6 min on the source). This resulted in a total integration time of 2 h spent on SNR 4449–1. A bright and relatively compact radio source, 4C +39.25, was observed as a fringe finder and bandpass calibrator.

The data were recorded in dual-circular polarization, at a rate of 1024 megabit per second (Mbps), resulting in a total bandwidth of 256 MHz (comprising eight intermediate frequency bands, each covering a 16 MHz band split into 32 spectral channels). After the observations, the data were correlated at the EVN Correlator Facility at JIVE[4] using a correlator averaging time of 2s. This ensured that the target source could be effectively detected within the 3σ error box of the VLA FIRST position measurement.

The correlated data were fringe-fitted using the AIPS[5] and phase solutions obtained on the phase-reference calibrator J1221+4411 were applied to the target source. No ionospheric corrections were applied. The target was subsequently imaged using the AIPS task IMAGR. The resulting image is shown in Fig. 1 and discussed below.

3   RESULTS

A phase-referenced image of SNR 4449–1 shown in Fig. 1 is obtained by applying CLEAN deconvolution to the naturally weighted data. The cleaning is done without self-calibration. The resulting restoring beam (CLEAN beam) is 7.9 mas × 3.5 mas, oriented at a position angle of 25°.8. The image has an off-source rms noise of 42 μJy beam^{-1} and a peak flux density of 287 μJy beam^{-1}, thus corresponding to a detection of signal-to-noise ratio (S/N)≈ 7.

The remnant is clearly resolved into several "spot-like" components, which is likely to reflect the limitations of deconvolution applied to visibility data with an incomplete *uv*-coverage due to the short integration time on the source (see Fig. 2). This effect may also contribute to the apparent discrepancy between the image in Fig. 1 and the structure observed with the

---
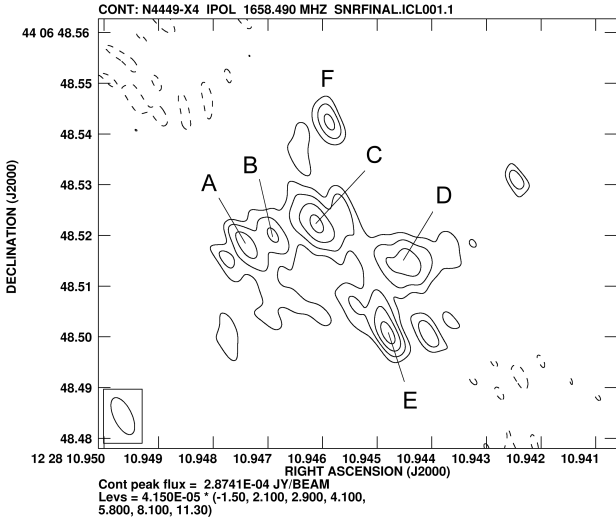
Figure 1. Resolved radio structure of the SNR in NGC 4449 using the EVN at 1.6 GHz. The rms noise off-source is $42\,\mu$Jy beam^{-1}. Contours start at -1.5 times the rms and increase with factors of $\sqrt{2}$. The six components detected are labelled A, B, C, D, E and F. The brightness peak of the map corresponds to component E and is 0.287 mJy beam^{-1}. The dimensions (full width at half-maximum) of the restoring beam are 7.9 mas×3.5 mas, with the major axis of the beam oriented along a position angle of 25°.8. North is up and east is to the left.

HSA[6] at 1.4 GHz by Bietenholz et al. (2010). The total flux density and the spatial extent of the radio emission are similar in both the 1.4 GHz HSA image and the 1.6 GHz one.

The most likely factor contributing to the morphological discrepancy is the difference of the baseline sensitivity and filling factors of the *uv*-coverages in the two data sets. The 1.4 GHz HSA data have a better rms noise resulting from a longer integration time and a superior *uv*-coverage on long baselines. However, the 1.6 GHz EVN observations have better coverage and better sensitivity on baselines shorter than 1000 km, which enhances detection of emission on angular scales of ∼35 mas. Making a firm conclusion on the structure of this SNR would require obtaining a robust *uv*-coverage on baselines of ⩽ 1000 km which can be provided by eMERLIN.

Six distinct regions (labelled A through F in Fig. 1) can be identified in the image. The basic properties of components A–F (coordinates, total flux densities, and brightness temperatures) have been obtained from fits by two-dimensional Gaussian components to the image plane. Table 2 lists the parameters obtained. The errors are taken from the covariance matrix of the fits.

The integrated flux density of the components identified varies from 0.269 to 0.648 mJy while the brightness temperature ranges from 3.0×10^6 to 5.6×10^6 K. The whole structure has a total flux of 6.1 ± 0.6 mJy, from which we derive a radio luminosity at 1.6 GHz of 1.74×10^{35} erg s^{-1}.

Component F is detected at an S/N∼ 5, while an even fainter component of 0.150 mJy of integrated flux is also present in the image, to the north-west from component D. These components are likely to be spurious features resulting from a sidelobe or deficiencies of the CLEAN convolution. In order to check the
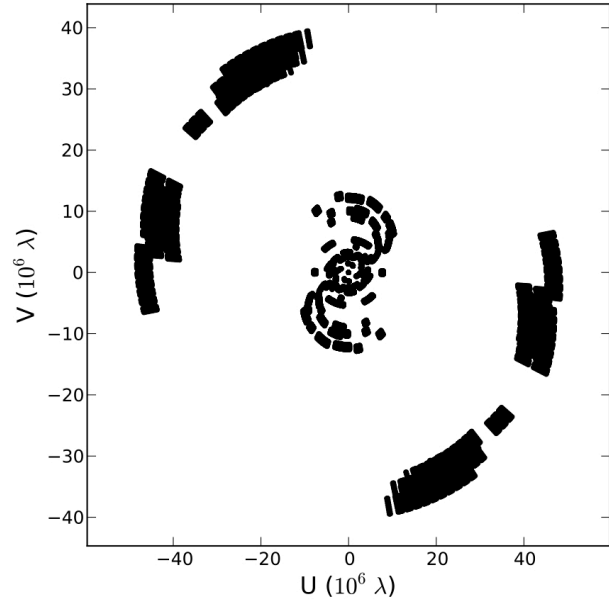
Figure 2. *uv*-coverage for an integration time of 2 hours on SNR 4449-1.

reliability of such components, we investigate variations in the deconvolution and data weighting schemes. We first repeat the data calibration and, in order to improve the image fidelity, split the data without applying any frequency averaging. We then perform CLEAN deconvolution using natural weighting and uniform weighting. The resulting images have off-source rms noises of 37 and 39 μJy beam^{-1} (see Fig. 3, left and right, respectively), and show a resolved structure formed by several spot-like components similar to those of Fig. 1. Some of the components previously observed are not detected here (e.g., component A seems to have merged with B), while the previous possible spurious detection of component F seems to be still detected at an S/N∼ 5. Despite the improvement in the image sensitivity, the structure of both images still shows an elliptical shape caused by the spatial frequencies sampled by the interferometer (see a further discussion on the image fidelity in the Appendix).

3.1 Positional centre and size of the remnant

The positional centre and an estimate of the SNR diameter size can be determined from the resolved structure. The fit of an ellipse to the structure formed by the peak of the five brightest components A-E (Fig. 4) yields the best position for the SNR centre at RA = $12^h28^m10^s.9463 \pm 0^s.0001$, Dec. = $44°06'48''.508 \pm 0''.001$, and a SNR size of major axis $b = 0.0422$ arcsec $\pm$ 0.0023 arcsec and minor axis $a = 0.0285$ arcsec $\pm$ 0.0024 arcsec corresponding to 0.8 pc × 0.5 pc at the distance of the galaxy. This estimate is limited by the uncertainty in the distance to NGC 4449. In order to compare the radio diameter to the one derived from optical images, we derive a geometrical mean value of 0.0347 arcsec $\pm$ 0.0025 arcsec. This size is larger than the value of 0.028 arcsec (Blair & Fesen 1998) and very similar to the 0.037 arcsec (Milisavljevic & Fesen 2008) estimated from the *HST* images, suggesting that the outer layers of SNR 4449–1 do also emit at optical wavelengths. The SNR mean diameter of 35 mas is larger than the ∼30 mas peak-to-peak separation between the two bright parallel ridges of emission found by Bietenholz et al. (2010). If
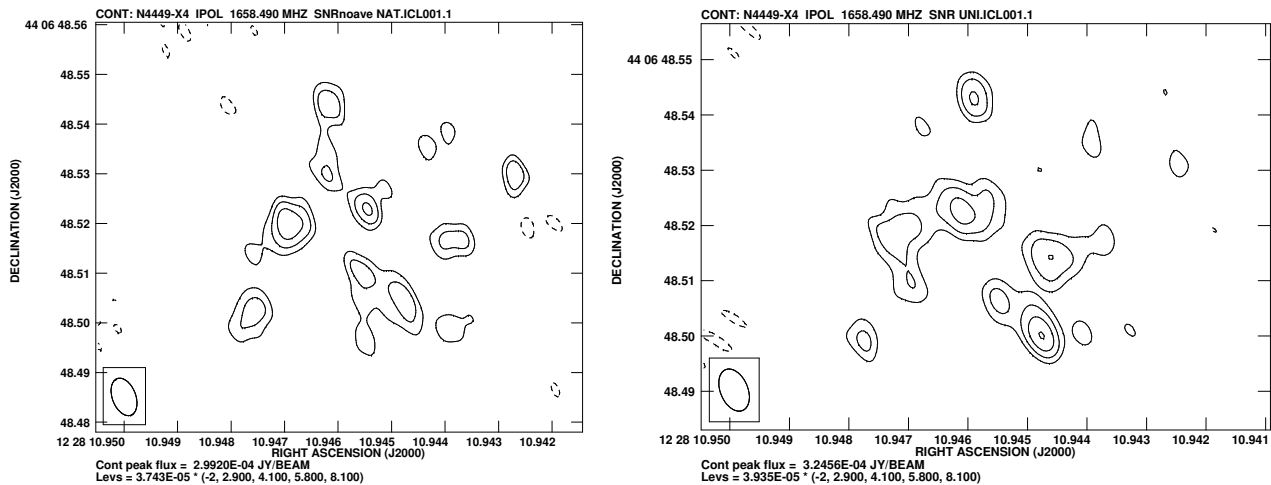
Figure 3. Resolved radio structure of the SNR in NGC 4449 using non-frequency averaged data. Left: deconvolved image using natural weighting. The rms noise off-source is $37\,\mu$ Jy beam^{-1} and the size of the restoring beam is 7.9 mas×4.7 mas, at a position angle of $20°.8$. Right: deconvolved image using uniform weighting. The rms noise off-source is $39\,\mu$ Jy beam^{-1} and the size of the restoring beam is 8.0 mas×5.0 mas, at a position angle of $22°.8$. The contours start at -1.5 times the rms and increase with factors of $\sqrt{2}$. North is up and east is to the left.

Table 2. Radio components of the SNR in NGC 4449

Component	RA (J2000)	Dec. (J2000)	Integrated flux (mJy)	$T_{\rm B}$ (10^6 K)
A	$12^h 28^m 10^s.94738 \pm 0^s.00006$	$44°06'48''.5181 \pm 0''.0008$	0.524	3.8
B	$12^h 28^m 10^s.94691 \pm 0^s.00006$	$44°06'48''.5200 \pm 0''.0008$	0.423	3.1
C	$12^h 28^m 10^s.94611 \pm 0^s.00003$	$44°06'48''.5223 \pm 0''.0004$	0.648	5.6
D	$12^h 28^m 10^s.94444 \pm 0^s.00005$	$44°06'48''.5146 \pm 0''.0007$	0.592	3.5
E	$12^h 28^m 10^s.94481 \pm 0^s.00003$	$44°06'48''.5008 \pm 0''.0005$	0.424	4.5
F	$12^h 28^m 10^s.94588 \pm 0^s.00004$	$44°06'48''.5423 \pm 0''.0007$	0.269	3.0

the component F also belongs to the remnant (as suggested in Bietenholz et al. 2010), the size of the remnant can be determined from the distance between components A–D and F–E. This yields a size of 32 mas × 43 mas, agreeing better with the size obtained by Bietenholz et al. (2010). It should be stressed here once more that deviations from the expected circular or elliptical morphology reported by Bietenholz et al. (2010) for SNR 4449–1 are not likely to result from deconvolution errors or gaps in the *uv*-coverage. These deviations (and the morphological discrepancy of the HSA and the EVN images of the remnant) most likely result from the deficiency in the structural sensitivity of both data sets for scales larger than $\sim$ 20 mas. While peculiar non-circular structures have also been observed in other SNRs (e.g., 41.95+575 in M82; McDonald et al. 2001), the apparent discrepancy of the structural appearance of the SNR in our image and the image of Bietenholz et al. (2010) calls for further more detailed imaging of this SNR.

4 DISCUSSION

4.1 Light curve

Using archival radio observations of NGC 4449, Lacey et al. (2007) presented the light curves of the SNR at 6 and 20 cm from 1972 to 2002 revealing a remarkable decline in its radio emission. An up-to-date version of the light curves, including the new flux
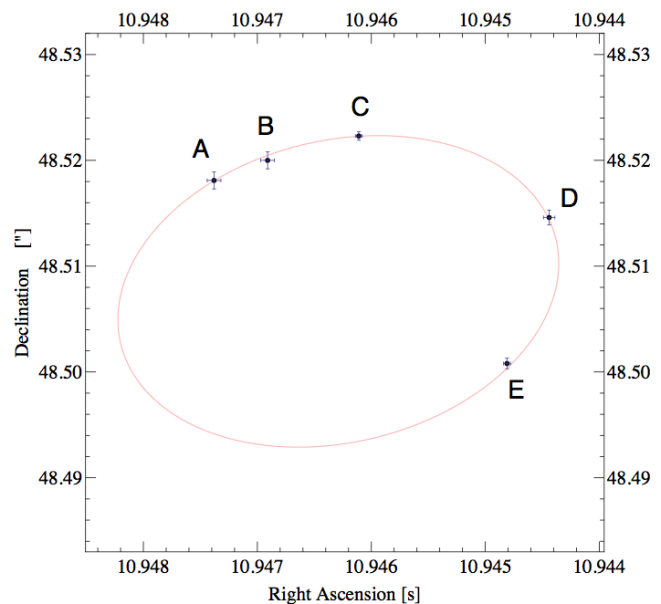
Figure 4. Elliptical fit to the peak of the five components detected. The ellipse has a major axis of 0.0422 arcsec $\pm$ 0.0023 arcsec, a minor axis of 0.0285 arcsec $\pm$ 0.0024 arcsec, and a position angle of $119°$. This corresponds to an ellipse of 0.8 pc × 0.5 pc.
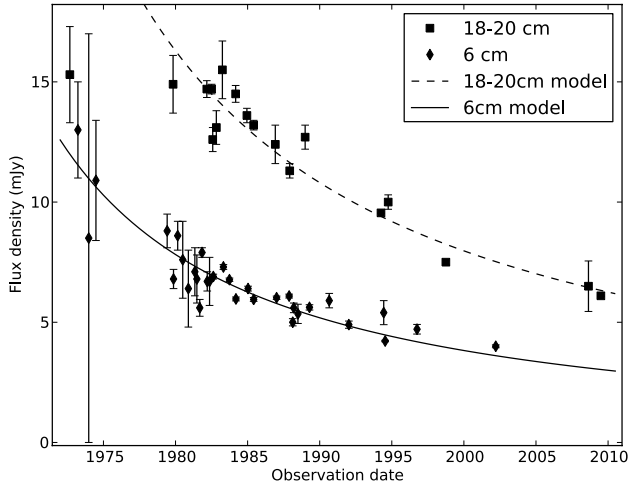
Figure 5. Lightcurve of SNR 4449–1 at 18 cm and 20 cm (squares), and 6 cm (diamonds). Data are taken from Lacey et al. (2007), Bietenholz et al. (2010), and this work. The dashed line (thick line) represents our best-fitting model to the 18–20 cm (6 cm) data using equation 1. Flux density measurements are treated separately at all three wavelengths. For presentation purposes, the 18 and 20 cm flux densities are plotted with the same symbol.

densities from Bietenholz et al. (2010) and this work, is presented in Fig. 5.

Our flux density measurement is in agreement with the radio decline and we use it to estimate the decay rate of the emission from a power-law fit of the form

$$S = S_0 (t - t_0)^\beta \nu^\alpha \,, \qquad (1)$$

where t_0 is the date of the SN explosion, S_0 is a scaling factor, ν is the observing frequency, α is the spectral index, and β is the index of the power-law decay (see, e.g., Weiler et al. 2002). From a combined fit to the lightcurves at 20, 18 and 6 cm (dashed and solid lines, Fig. 5), we obtain $S_0 = 922 \pm 307$ Jy, $t_0 = 1956 \pm 2$ yr (AD), $\beta = -1.19 \pm 0.07$, and $\alpha = -0.620 \pm 0.004$, with a $\chi^2 = 9$.

The value of β obtained from this fit yields a secular decline rate of the radio emission of $2.2 \pm 0.1 \%$ per year. This decline rate is similar to the ones found for SN 1970G in the periods 1973–1991 and 1991–2001 (Cowan et al. 1991; Stockdale et al. 2001), and it is slightly lower than the value 2.8% obtained by Lacey et al. (2007) under the assumption of the SNR age of ~ 100 yrs.

Lacey et al. (2007) report variations of the spectral index, α, observed over the time period 1972–2002. The spectral index remains relatively constant from 1982 to 1996, with an average value of $\alpha \approx -0.65$ obtained largely from 1.4 and 4.8 GHz measurements. This value is in good agreement with the spectral index derived from our combined fit to the light curves at 6 and 20 cm. It steepens later to $\alpha \approx -1$, albeit in measurements involving 22 GHz where spectral aging is more pronounced.

4.2 Constraining the age of SNR 4449–1

The estimate of $t_0 \sim 1956$ yr (AD) indicates that the SN should have exploded ~ 55 yr ago. This age agrees with the upper limit of 100 years (Milisavljevic & Fesen 2008) and with the ~ 70 yr suggested by Bietenholz et al. (2010). It is also in agreement with the detections of the SNR on optical plates (see Milisavljevic &

Fesen 2008 for a discussion), which indicated that the SN explosion must have taken place in 1961 or before.

Using the [OIII] optical emission line of the SNR spectrum, a range of expansion speeds of the SNR of 3000-6000 km s^{-1} was found (Blair & Fesen 1998). An estimated maximum expansion velocity of ~ 6500 km s^{-1} was later provided (Bietenholz et al. 2010). This velocity range can be used to derive a lower limit on the age of SNR 4449–1. Adopting the SNR radius of 14–21 mas, as given by the semimajor and semiminor axes of the elliptical fit shown in Fig. 4 and an expansion speed of ~ 6500 km s^{-1}, we estimate an age of the SNR between 39 and 59 yr (assuming a constant expansion speed). The SN explosion would thus have taken place between 1951 and 1971, which is in agreement with the $t_0 \sim 1956$ found from the fit to the radio light curves. Adopting an SNR radius of 16–21 mas, as given by the size estimate made with the feature F included, we obtain an age of the SNR of between 44 and 60 yr. This constrains the year of the SN explosion between 1950 and 1965, which is also in agreement with $t_0 \sim 1956$.

We note that these estimates are made under the assumption that the radio shell is expanding together with the optical [OIII] emitting gas, at a constant speed of ~ 6500 km s^{-1}. This is supported by the finding that the size of the shell-like structure observed at 1.6 GHz is similar to the one in the optical. If the outer shock front were moving faster than 6500 km s^{-1}, the ages estimated using this expansion speed would constitute an upper limit to the remnant's age.

Decelerated expansion

A deceleration in the shock front, produced by the interaction of the ejecta with a dense CSM, would affect the estimated age of the SNR as well. Chevalier (1982a,b) proposed that the relativistic electrons and enhanced magnetic field necessary to produce the observed radio synchrotron emission arise from the SN shock wave interacting with a dense CSM, which is presumed to have been established by a very effective mass-loss wind from the SN stellar progenitor.

According to Chevalier (1982a,b), the shock front of the SN in the CSM expands following a power law of time, $r \propto t^m$, where m is the *deceleration parameter* defined as

$$m = (n - 3)/(n - s) \,. \qquad (2)$$

The radial density profiles of the ejecta and the CSM are also described as power laws, with indices n and s, respectively (i.e., the ejecta density is $\propto r^{-n}$ and the CSM density is $\propto r^{-s}$). The deceleration parameter, m, can also be written in terms of the spectral index, α, and the flux-density decay rate, β, in the form (see Martí-Vidal et al. 2011b)

$$m = \frac{2(3 + \alpha + \beta)}{3(s - 4) + \alpha(s - 2)} \,. \qquad (3)$$

Taking the values of $\alpha = -0.62$ and $\beta = -1.19$, estimated from our fit to the radio light curves, equation 3 results in a deceleration parameter $m = 0.80$, if we use a radial CSM profile with $s = 2$ (i.e., if we assume a constant mass-loss rate for the progenitor star). This value is in agreement with the typical values reported in other SNe (where the expansion has been monitored during several years). It is found in all cases that $0.7 \leqslant m \leqslant 0.9$ (Bietenholz et al. 2002; Weiler et al. 2002; Marcaide et al. 2009; Martí-Vidal et al. 2011a; and references therein).

5 SUMMARY

We have presented the shell-like resolved structure of the young oxygen-rich SNR in NGC 4449. We obtain the most accurate estimates of the SNR position and size (0.0422 arcsec × 0.0285 arcsec, corresponding to 0.8 pc × 0.5 pc at a distance of 3.82 Mpc), making this object one of the largest extragalactic SNRs imaged with VLBI. The historical light curve of the source can be well fitted by a power law of index $\beta = -1.19 \pm 0.07$, after the inclusion of the total flux density at 1.6 GHz, and an SNR age of ~ 55 yr. A decline rate of the radio emission of $\mathrm{d}S/S\mathrm{d}t = -(2.2 \pm 0.1)\,\%$ yr^{-1} is found.

According to the fit of the radio light curves, the SN should have exploded around 1956, which is in agreement with the detection of the SN in the optical plates and with the age obtained assuming linear expansion with a maximum speed derived from the optical oxygen lines of ~ 6500 km s^{-1}. The constraint of the explosion date of SNR 4449–1 places this source in a unique position as being the youngest known supernova remnant (Cas A is the youngest Galactic SNR with an age of ~ 330 yrs; Thorstensen et al. 2001).

From the 1.6 GHz VLBI observation, we derive a luminosity of 1.74×10^{35} erg s^{-1}, which is comparable to the peak luminosity of SN 1970G and higher than the current luminosities of the Galactic SNRs Cas A and the Crab (see Lacey et al. 2007 for further discussion). This makes SNR 4449–1 an interesting link between SNe and their remnants and calls for classifying this object as a transition-type source that links SN explosions and SNRs (Lacey et al. 2007) or as an intermediate-age SNR with an exceptionally high radio luminosity (the so-called 'radio hypernova remnant'; Wilkinson & de Bruyn 1990).

Additional monitoring at multiple radio frequencies is required to refine the fractional decline rate, light curve and spectral index evolution of the SNR, and to determine its properties and classification.

REFERENCES

Annibali F., Aloisi A., Mack J., Tosi M., van der Marel R. P., Angeretti L., Leitherer C., Sirianni M., 2008, AJ, 135, 1900
Balick B., Heckman T., 1978, ApJ, 226, L7
Bietenholz M. F., Bartel N., Milisavljevic D., Fesen R. A., Challis P., Kirshner R. P., 2010, MNRAS, 409, 1594
Bietenholz M. F., Bartel N., Rupen M. P., 2002, ApJ, 581, 1132
Blair W. P., Fesen R. A., 1998, in BAAS. p. 1365
Blair W. P., Kirshner R. P., Winkler Jr. P. F., 1983, ApJ, 272, 84
Chevalier R. A., 1982a, ApJ, 259, L85
Chevalier R. A., 1982b, ApJ, 259, 302
Cowan J. J., Goss W. M., Sramek R. A., 1991, ApJ, 379, L49
de Bruyn A. G., 1983, A&A, 119, 301
Eck C. R., Roberts D. A., Cowan J. J., Branch D., 1998, ApJ, 508, 664
Heywood I., Blundell K. M., Klöckner H.-R., Beasley A. J., 2009, MNRAS, 392, 855
Lacey C. K., Goss W. M., Mizouni L. K., 2007, AJ, 133, 2156
Liu J.-F., Bregman J. N., 2005, ApJS, 157, 59
Marcaide J. M., Martí-Vidal I., Perez-Torres M. A., Alberdi A., Guirado J. C., Ros E., Weiler K. W., 2009, A&A, 503, 869
Martí-Vidal I., Marcaide J. M., Alberdi A., Guirado J. C., Pérez-Torres M. A., Ros E., 2011, A&A, 526, A142
Martí-Vidal I., Pérez-Torres M. A., Brunthaler A., 2011, A&A, 529, A47
McDonald A. R., Muxlow T. W. B., Pedlar A., Garrett M. A., Wills K. A., Garrington S. T., Diamond P. J., Wilkinson P. N., 2001, MNRAS, 322, 100
Mezcua M., Farrell S. A., Gladstone J. C., Lobanov A. P., 2013, MNRAS, preprint (arXiv:1309.4463)
Mezcua M., Lobanov A. P., 2011, Astron. Nachr., 332, 379
Milisavljevic D., Fesen R. A., 2008, ApJ, 677, 306
Pennington R. L., Dufour R. J., 1983, ApJ, 270, L7
Reines A. E., Johnson K. E., Goss W. M., 2008, AJ, 135, 2222
Sánchez-Sutil J. R., Muñoz-Arjonilla A. J., Martí J., Garrido J. L., Pérez-Ramírez D., Luque-Escamilla P., 2006, A&A, 452, 739
Seaquist E. R., Bignell R. C., 1978, ApJ, 226, L5
Stockdale C. J., Goss W. M., Cowan J. J., Sramek R. A., 2001, ApJ, 559, L139
Summers L. K., Stevens I. R., Strickland D. K., Heckman T. M., 2003, MNRAS, 342, 690
Thorstensen J. R., Fesen R. A., van den Bergh S., 2001, AJ, 122, 297
Weiler K. W., Panagia N., Montes M. J., Sramek R. A., 2002, ARA&A, 40, 387
Wilkinson P. N., de Bruyn A. G., 1990, MNRAS, 242, 529
Yokogawa J., Imanishi K., Koyama K., Nishiuchi M., Mizuno N., 2002, PASJ, 54, 53

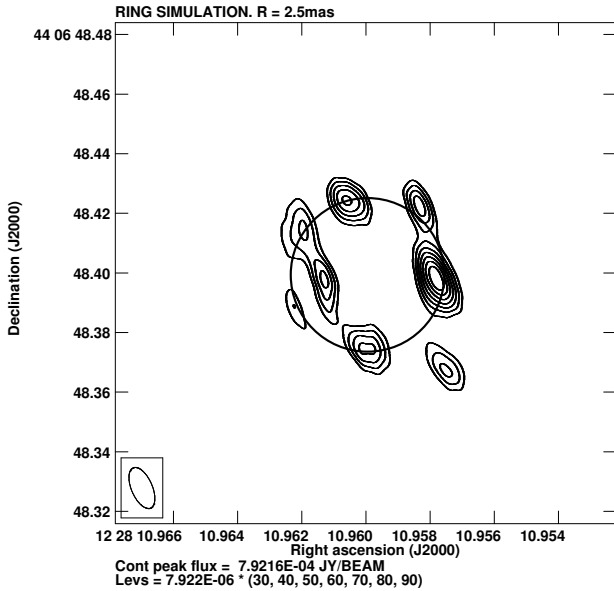## APPENDIX

Discussion on the image fidelity

The sparse *uv*-coverage of our observations has a direct effect on the fidelity of the SNR N4449−1 image. Holes in the *uv*-coverage map into a complete filtering of a range of spatial frequencies in the image plane. Hence, any structure with spatial scales corresponding to spatial frequencies not covered in our observations will be invisible to the interferometer.

On the one hand, extended sources (like spherical shells or rings) have different amplitude components at different spatial scales. If we are unable to measure all these components at all spatial frequencies, it is difficult (if not impossible) to recover the source structure with a high fidelity, unless some assumptions are made. On the other hand, things are different for sources consisting of a discrete set of compact (i.e., point-like) components. A point source has exactly the same amplitude at all the spatial scales. Hence, the imaging of such a source (or a discrete set of such sources) is very robust, even if the *uv*-coverage is sparse.

Our image of SNR N4449−1 consists of a set of compact sources distributed following a somewhat elliptical manner. This image can be understood as an elliptical structure, whose spatial frequencies have been filtered by a sparse *uv*-coverage. As a result of the spatial-frequency filtering, the image is only

RING SIMULATION. R = 2.5mas

Cont peak flux = 7.9216E-04 JY/BEAM
Levs = 7.922E-06 * (30, 40, 50, 60, 70, 80, 90)

Figure 6. Contour plot of the deconvolved image of a spherical shell, of size 50 mas, obtained from a realistic simulation of our EVN observations (see the text). The thick circle line marks the outer radius of the simulated shell.

sensitive to the portions of the elliptical structure whose spatial frequencies are sampled by the interferometer. The effect of a sparse *uv*-coverage on extended sources (in particular, the shell-like structures corresponding to radio-SNRs) was studied by Heywood et al. (2009) and discussed (and discarded) in Bietenholz et al. (2010) as a possible origin of the distorted structure seen in their HSA image of SRN N4449−1.

We have performed a test similar to that described in Bietenholz et al. (2010), although with some substantial differences. Instead of simulating observations of a spherical shell from a synthetic *uv*-coverage and receiver noise, we added the shell model to the residual (i.e., post-CLEAN) visibilities of our own observations. This way, the noise and the visibility weights result to be *exactly* the same as those of the real source observations. The deconvolved image of the spherical shell (of size 50 mas) is shown in Fig. 6. The recovered signal from the shell is broken into several compact features, which are distributed around the outer edge of the source structure. Hence, if the structure of SNR N4449−1 is extended (as it is indeed the case), our sparse *uv*-coverage translates into an incomplete detection of the whole structure, with several compact components distributed along the radio-emitting region. Hence, it is not possible to discern the innermost details of the source structure from our observations (i.e., we cannot tell whether the source resembles more a disc, a ring, or a shell), but we can still get information on the source size, based on the distribution of the compact components recovered in our image.